The Seismic Record
A journal of the Seismological Society of America

Back-Azimuth Estimation of Air-to-Ground Coupled Infrasound from Transverse Coherence Minimization

Jordan W. Bishop[*1,2], Matthew M. Haney[3], David Fee[1], Robin S. Matoza[4], Kathleen F. McKee[5], and John J. Lyons[3]

Abstract

We present the transverse coherence minimization method (TCM)—an approach to estimate the back-azimuth of infrasound signals that are recorded on an infrasound microphone and a colocated three-component seismometer. Accurate back-azimuth information is important for a variety of monitoring efforts, but it is currently only available for infrasound arrays and for seismoacoustic sensor pairs separated by 10 s of meters. Our TCM method allows for the analysis of colocated sensor pairs, sensors located within a few meters of each other, which may extend the capabilities of existing seismoacoustic networks and supplement operating infrasound arrays. This approach minimizes the coherence of the transverse component of seismic displacement with the infrasound wave to estimate the infrasound back-azimuth. After developing an analytical model, we investigate seismoacoustic signals from the August 2012 Humming Roadrunner experiment and the 26 May 2021 eruption of Great Sitkin Volcano, Alaska, U.S.A., at the ranges of 6.5–185 km from the source. We discuss back-azimuth estimates and potential sources of deviation (1°–15°), such as local terrain effects or deviation from common analytical models. This practical method complements existing seismoacoustic tools and may be suitable for routine application to signals of interest.

Cite this article as Bishop, J. W., M. M. Haney, D. Fee, R. S. Matoza, K. F. McKee, and J. J. Lyons (2023). Back-Azimuth Estimation of Air-to-Ground Coupled Infrasound from Transverse Coherence Minimization, *The Seismic Record*. **3**(**4**), 249–258, doi: 10.1785/0320230023.

Supplemental Material

Introduction

Infrasound waves, sound waves with frequencies below ~20 Hz, induce ground motion when they impinge on the Earth's surface. These signals are commonly observed on vertical and horizontal components of seismometers (Johnston, 1987), in which they are sometimes called ground-coupled airwaves (GCAs). Acoustic waves at grazing incidence couple into the ground along the vertical and radial components of the propagation path, and analytical models predict a $-\pi/2$ phase shift between the incident acoustic wave and the vertical component of the seismic velocity (e.g., Sorrells, 1971; Ben-Menahem and Singh, 1981; Anthony, Ringler, *et al.*, 2022). Acoustic-seismic energy transfer is complex and dependent on many factors, including arrival angle and elastic medium parameters (Bishop *et al.*, 2022). GCAs have been recorded from a variety of natural (McKee *et al.*, 2018) and anthropogenic phenomena (Edwards *et al.*, 2007), and further development of GCA analysis methods may provide additional constraints on acoustic source location (Assink *et al.*, 2016) as well as Earth structure at the sensor locations (Anthony, Ringler, *et al.*, 2022).

After an infrasound signal is detected on a collection of sensors (Fee *et al.*, 2016), accurately estimating the signal back-azimuth is an important step for a variety of monitoring frameworks (Matoza *et al.*, 2017; Blom *et al.*, 2020). Multiple methods have been developed to identify GCAs in seismic data

1. Wilson Alaska Technical Center, Geophysical Institute, University of Alaska Fairbanks, Fairbanks, Alaska, U.S.A., https://orcid.org/0000-0002-8940-9827 (JWB); https://orcid.org/0000-0002-0936-9977 (DF); 2. Now at Los Alamos National Laboratory, Los Alamos, New Mexico, U.S.A.; 3. U.S. Geological Survey, Alaska Volcano Observatory, Anchorage, Alaska, U.S.A., https://orcid.org/0000-0003-3317-7884 (MMH); https://orcid.org/0000-0001-5409-1698 (JJL); 4. Department of Earth Science and Earth Research Institute, University of California, Santa Barbara, California, U.S.A., https://orcid.org/0000-0003-4001-061X (RSM); 5. Department of Earth and Environmental Sciences, Vanderbilt University, Nashville, Tennessee, U.S.A., https://orcid.org/0000-0003-3189-9189 (KFM)

*Corresponding author: jwbishop@lanl.gov

© 2023. The Authors. This is an open access article distributed under the terms of the CC-BY license, which permits unrestricted use, distribution, and reproduction in any medium, provided the original work is properly cited.

Downloaded from http://pubs.geoscienceworld.org/ssa/tsr/article-pdf/3/4/249/5979003/tsr-2023023.1.pdf
by guest

using an infrasound sensor and a nearby seismometer (Ichihara *et al.*, 2012; Matoza and Fee, 2014; Mendo-Pérez *et al.*, 2021). These methods complement seismic polarization analysis and better enable wavefield separation (Haney *et al.*, 2020). For example, ground motion from volcanic eruptions may be due to seismic tremor or sustained infrasonic signals (Matoza and Fee, 2014). The coherence between the infrasound data and the vertical component of the seismometer is crucial for identifying frequencies that are from air-to-ground coupled waves instead of pure seismic waves. For nearly colocated infrasound and seismometer sensor pairs, in which seismometers and infrasound sensors are located within tens of meters from each other, the GCA-BAD determination method can be used to estimate the back-azimuth of the incident infrasound wave by leveraging the sensor separation and associated phase offset (McKee *et al.*, 2018). This method is useful but relies on sensors being separated by at least a few meters (5–212 m in the previous work)—a distance the infrasound signal propagates over several sample increments. In addition, a relatively high sample rate is required to accurately estimate the back-azimuth from time shifting, with the optimum recommended as ≥100 Hz (McKee *et al.*, 2018). To leverage a broader range of sensor configurations for signal back-azimuth estimation, such as data from the former USArray Transportable Array (TA; Busby and Aderhold, 2020), we seek a method for processing approximately colocated infrasound microphone and seismometer pairs.

Here, we introduce the transverse coherence minimization (TCM) method. We first briefly describe our approach and provide a derivation. We then analyze seismoacoustic signals from the August 2012 Humming Roadrunner (HRR) trials and the 26 May 2021 eruption of Great Sitkin Volcano, Alaska, U.S.A. Finally, we discuss some limitations to this technique and future work.

TCM

Analytical models suggest that acoustic waves only couple into the ground along the propagation path of the wave in the vertical and radial directions (Ben-Menahem and Singh, 1981). Because of the spatial symmetry in the pressure wave, there is no differential ground motion along the wavefront for flat ground and a horizontally layered Earth model. This also means that there is no differential displacement along the wavefront. Thus, the seismic velocity and displacement components normal to the vertical and radial directions, that is, the transverse component, are zero. Motivated by this theory, our TCM method works by estimating the signal direction such that the coherence between the infrasound and transverse component of the seismic data is minimized. In practice, both the azimuth and the back-azimuth minimize this coherence. In an effort to resolve this ambiguity, we choose the back-azimuth such that the resulting seismic particle motion is retrograde (McKee *et al.*, 2018).

Our method is based on the magnitude-squared coherence between an infrasonic signal (I) and seismically coupled transverse displacement (T):

$$C_{TI} = \frac{|TI^*|^2}{|T|^2|I|^2}. \tag{1}$$

For a given frequency, we denote the complex conjugate of the infrasound signal Fourier coefficient as I^*. We further develop this model by assuming that the infrasound wave and seismic displacement recorded on the north (N) and east (E) components of the seismometer can be expressed as harmonic plane waves with uncorrelated noise.

$$\begin{aligned} I &= A_I e^{i(\omega t+\phi_I)} + n_I, \\ \mathrm{E} &= A_R \sin\psi e^{i(\omega t+\phi)} + n_\mathrm{E}, \\ \mathrm{N} &= A_R \cos\psi e^{i(\omega t+\phi)} + n_\mathrm{N}, \end{aligned} \tag{2}$$

in which A_I is the infrasound amplitude; A_R is the amplitude of the radial seismic displacement; n_I is the infrasound noise; n_E is the east component seismic noise; n_N is the north component seismic noise; ψ is the infrasound back-azimuth; ω is the angular frequency; t is time; and ϕ is a phase angle. Although they are uncorrelated, we assume that the n_E and n_N have the same expected value, which we refer to generally as seismic noise (n). Moreover, we decompose the transverse seismic component into N and E components from a wave with a trial back-azimuth (θ):

$$T = \mathrm{N}\sin(\theta) - \mathrm{E}\cos(\theta). \tag{3}$$

Substituting equations (2) and (3) into equation (1) (see the supplemental material, available to this article), we simplify to obtain:

$$C_{TI}(\theta) = \frac{\sin^2(\theta-\psi)}{\left(1+\frac{n_I^2}{A_I^2}\right)\left(\sin^2(\theta-\psi)+\frac{n_r^2}{A_r^2}\right)}. \tag{4}$$

Equation (4) describes the transverse seismoinfrasonic magnitude-squared coherence as a function of the trial back-azimuth (θ). This transverse magnitude-squared

Downloaded from http://pubs.geoscienceworld.org/ssa/tsr/article-pdf/3/4/249/5979003/tsr-2023023.1.pdf
by guest

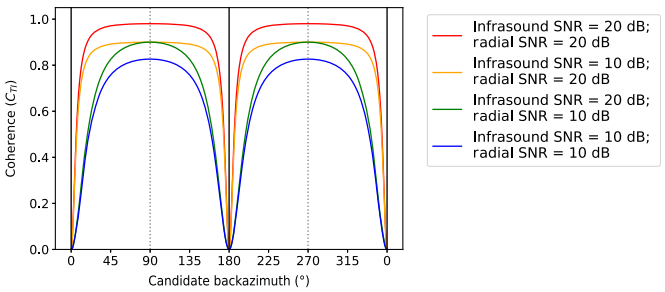

Figure 1. Magnitude-squared coherence model ($C_{TI}(\theta)$) for different infrasound and radial seismic signal-to-noise ratios (SNRs; equation 4). The hypothetical signal back-azimuth (ψ) is 0°, so the transverse coherence has minima at 0° and 180° (black vertical lines). The corresponding radial coherence maxima occur at 90° and 270° (gray vertical dashed lines).

coherence ($C_{TI}(\theta)$) is zero when θ equals the back-azimuth (ψ) of the incident infrasound wave, and we note that equation (4) lacks an explicit frequency dependence. For computational speed, we use tensor rotations to form the spectral density matrices of the transverse component in equation (4) from spectral densities of the N and E seismic components. Throughout this work, we also use the magnitude-squared coherence between the infrasound microphone and the vertical seismic displacement (Z) both as a heuristic to denote relative quality in the arrival of the infrasound wave as well as a frequency-dependent weighting function:

$$C_{ZI} = \frac{|ZI^*|^2}{|Z|^2|I|^2}. \quad (5)$$

Example values of equation (4) with different signal-to-noise (SNR) levels (using peak-to-peak amplitudes) for the infrasound ($\frac{A_I^2}{n_I^2}$) and the radial seismic component ($\frac{A_R^2}{n^2}$) are shown in Figure 1. We see that the transverse coherence minima become sharper for larger SNR on the radial seismic component (compare red and green lines), thus the uncertainty in the estimate of the true back-azimuth decreases. We also note that the maxima of the curves (radial magnitude-squared coherence) in Figure 1 are much broader and more poorly defined than the minima (transverse magnitude-squared coherence). Furthermore, for the same seismic SNR, lowering the infrasound SNR appears to lower the peak radial coherence (compare red and orange lines), but it has no affect on the transverse minimum, because it acts as an overall scale factor in equation (4). For these reasons, we advocate for TCM instead of radial coherence maximization (Anthony, Ringler, *et al.*, 2022).

Data

To illustrate our method, we investigate seismoacoustic signals from the August 2012 HRR experiment and the 26 May 2021 explosive eruption of Great Sitkin Volcano.

HRR analysis

The HRR experiment consisted of a series of controlled chemical explosions at the White Sands Missile Range in New Mexico, U.S.A., from 14 to 31 August 2012 (Fig. 2a; Kim and Rodgers, 2017). The resulting infrasound was recorded at local-to-regional distances (Kim and Rodgers, 2017; Green *et al.*, 2018). We use the TCM method to estimate the back-azimuth of the infrasound signals recorded on TA station 121A (32.532398°, −107.785103°) from the HRR-1 and HRR-3 explosions in the series. This station is located 160 km from HRR-1 and 173 km from HRR-3. HRR-1 (33.41902°, −106.42937°) was an 18,140 kg trinitrotoluene (TNT)-equivalent explosion that occurred on 16 August 2012, and HRR-3 (33.68042°, −106.52276°) was a 9070 kg TNT equivalent explosion that occurred on 19 August 2012. For additional analysis of the infrasound recordings and propagation conditions from this experiment, we refer the reader elsewhere (Kim and Rodgers, 2017; Green *et al.*, 2018). An additional example showing TCM results for the HRR-1 signal recorded on TA station W18A is also provided in the supplemental material. TA station 121A had a Hyperion microbarometer, a Quantera 330 linear phase composite digitizer, and a colocated Streckeisen STS-2 G3 three-component seismometer. We filtered the infrasound and seismic waveforms from 10.0 to 17.0 Hz for HRR-1 and from 8.0 to 16.0 Hz for HRR-3. We process both the HRR-1 data and the HRR-3 data in 5 s windows with 90% overlap. For our back-azimuth estimation, we smooth the coherence over four adjacent windows as a form of regularization on the parameter estimates.

Great Sitkin Volcano eruption analysis

Seismic and infrasonic signals from the 26 May 2021 eruption of Great Sitkin Volcano (05:03:55.84 UTC) were recorded at multiple stations across the Alaska Volcano Observatory (AVO) monitoring network. Here we focus on seismoacoustic station pairs GSMY, GALA, KOWE, and KONW (Fig. 2b), which are located ~7 km (GSMY), 185 km (GALA), 132 km (KOWE), and 136 km (KONW) away from Great Sitkin Volcano. Each station pair is equipped with a Chaparral 64-UHP2 infrasound sensor, a Nanometrics Centaur digitizer, and a Trillium Compact 120 s three-component seismometer. The infrasound microphone

Downloaded from http://pubs.geoscienceworld.org/ssa/tsr/article-pdf/3/4/249/5979003/tsr-2023023.1.pdf
by guest

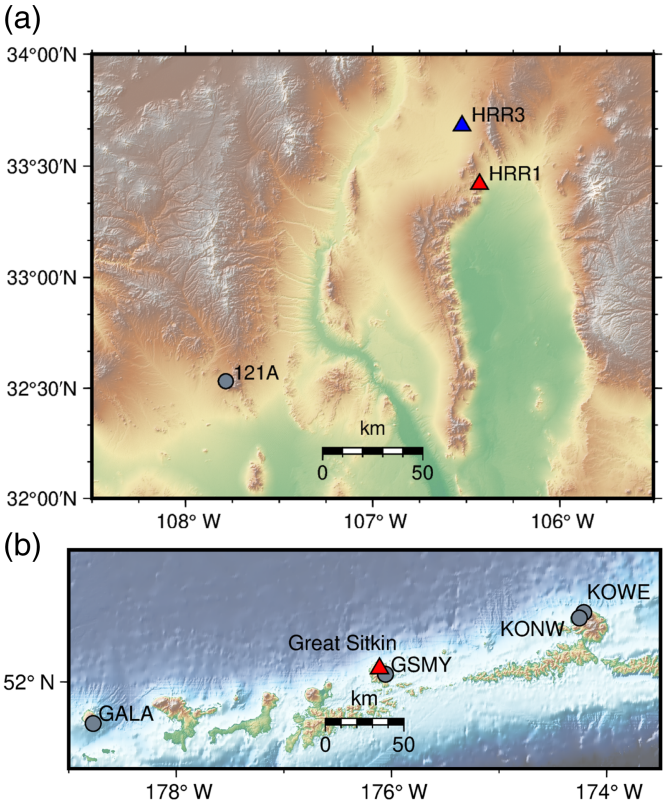

Figure 2. Map of the colocated infrasound and seismometer sensor pairs used in this study. (a) TA station 121A (gray marker) is shown to the southwest of Humming Roadrunner (HRR1; red triangle) and HRR3 (blue triangle). (b) Alaska Volcano Observatory (AVO) stations GSMY, GALA, KONW, and KOWE (gray markers) are shown in relation to Great Sitkin Volcano (red triangle).

and the three-component seismometer are located within ~10 m of each other for these stations. Data from GALA and GSMY are filtered from 13.0 to 18.0 Hz, and data from KOWE and KONW are filtered from 14.0 to 18.0 Hz. Data from all the four stations are processed in 5 s windows with 90% overlap. We again smooth the coherence over four adjacent windows for our back-azimuth estimation.

Results

HRR analysis

TCM processing results for the HRR-1 and HRR-3 explosions recorded on TA station pair 121A are shown in Figure 3. An impulsive infrasound signal from HRR-1 is visible at 18:19:28 UTC (Fig. 3a) and lasts for~5 s; notably the signal arrives in an otherwise noisy window (Fig. 3a,e). An impulsive seismic displacement signal with high coherence between the vertical seismic component and the infrasound signal is also observed (Fig. 3c,i). The TCM-derived back-azimuth estimates during this time start at ~55° with low coherence ($C_{ZI} = 0.47$) migrates to 53° at the maximum mean weighted coherence ($C_{ZI} = 0.85$) and then returns to ~57° with decreasing coherence ($C_{ZI} = 0.48$; Fig. 3k). The back-azimuth estimate at the maximum mean weighted coherence (53°) is deviated ~1° from the source back-azimuth (52°).

The infrasound data and TCM processing for 121A show up to four arrivals that may be associated with HRR-3 (Fig. 3). A low-amplitude signal first appears on the infrasound and seismic traces at 23:35:49, followed by an impulsive, higher amplitude signal at 23:36:01. Two other potential arrivals appear at 23:36:40 and 23:37:00 (Fig. 3b,f). The infrasound and vertical seismic traces have broad, high-magnitude-squared coherence (C_{ZI}) across this time period (Fig. 3l,p). Back-azimuth estimates starting at 23:35:49 are between 53° and 56°, with a peak at coherence ($C_{ZI} = 0.55$) at ~49°. For the signal beginning at 23:36:01, the back-azimuth estimates start at ~38° and migrate to 54° with a relatively high coherence ($C_{ZI} > 0.70$). This signal has the highest vertical coherence ($C_{ZI} = 0.85$), and the associated back-azimuth value (39°) is deviated ~3° from the ground-truth back-azimuth to the HRR-3 explosion. The signal at 23:36:40 has back-azimuth estimates that range from 53° to 34° with a mean vertical magnitude-squared coherence of 0.47, and the back-azimuth estimates for the signal at 23:37:00 ranges from 55° to 33° with a mean vertical magnitude-squared coherence of 0.51.

To more directly connect our time–frequency processing with our analytical model (Fig. 1), Figure 3o,p shows the transverse coherence (equation 1) calculated by rotating a 5 s window of infrasound and horizontal seismic data for HRR-1 and HRR-3. These data were filtered in the same frequency band as the TCM processing, and the time windows are marked by the blue shaded regions in (Fig. 3a–d). As suggested by our analytical model (Fig. 1), both the plots have transverse minima that are narrower than their radial coherence maxima. However, the coherence plot for HRR-3 also has local minima in the transverse coherence at 67° and 247°. When looking at the time–frequency plots of transverse coherence (Fig. 3m,n), we likewise see that the transverse coherence for HRR-1 is low across the frequencies of interest, but HRR-3 data has higher (>0.50) transverse coherence across some frequencies. When the seismic data are rotated using the ground-truth back-azimuth, the spectrograms for the transverse components show little energy (Fig. 3g,h). The transverse coherence does not

Downloaded from http://pubs.geoscienceworld.org/ssa/tsr/article-pdf/3/4/249/5979003/tsr-2023023.1.pdf
by guest

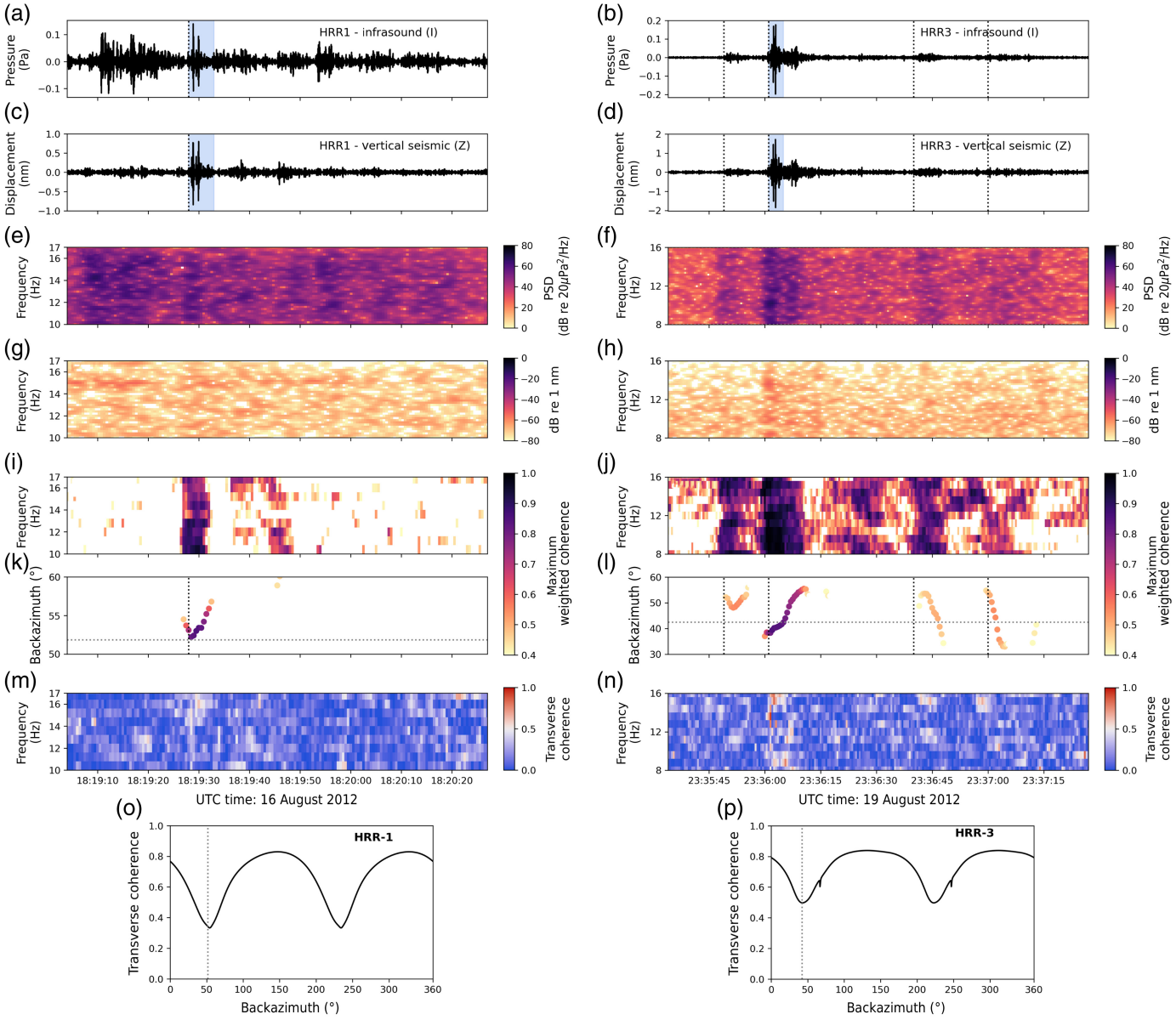

go to zero, as suggested by our analytical model (equation 4). In deriving our model, we assume that our infrasound and horizontal seismic noise variables are uncorrelated. However, correlation between infrasound and horizontal seismic components can occur for ground tilt (Dybing *et al.*, 2019).

Great Sitkin Volcano eruption analysis

TCM processing results for regional stations GALA and GSMY are shown in Figure 4. Seismoacoustic station GALA (Fig. 2b) records a clear infrasound signal and GCA at ~05:14:58 UTC (Fig. 4a,c,e). The vertical magnitude-squared coherence is highly variable across the analysis frequency band (Fig. 4i). Back-azimuth estimates generally point in the direction of

Figure 3. Transverse coherence minimization method (TCM) analysis of the HRR-1 (a,c,e,g,i,k,m,o) and HRR-3 (b,d,f,h,j,l,n,p) signals recorded at TA station 121A. TCM processing results are (a,b) the pressure trace from the infrasound sensor; (c,d) the vertical seismic displacement; (e,f) the infrasound spectrogram; (g,h) the spectrogram of the transverse seismic component; (i,j) the magnitude-squared coherence between the infrasound and vertical displacement (equation 5); (k,l) the back-azimuth estimates; and (m,n) the transverse coherence. The transverse spectrogram is calculated using the ground-truth back-azimuth to the source, and the transverse coherence is obtained by rotating the horizontal seismic components using the back-azimuth estimates in panels (k) and (l). For comparison with Figure 1, we show the transverse coherence from a rotation of the broadband seismic waveforms in panels (o) and (p). The blue shaded 5 s regions in the infrasound and seismic traces were chosen for rotation. The gray dotted lines in panels (k,o) and (l,p) indicate the geographic back azimuths to HRR-1 and HRR-3, respectively.

Downloaded from http://pubs.geoscienceworld.org/ssa/tsr/article-pdf/3/4/249/5979003/tsr-2023023.1.pdf
by guest

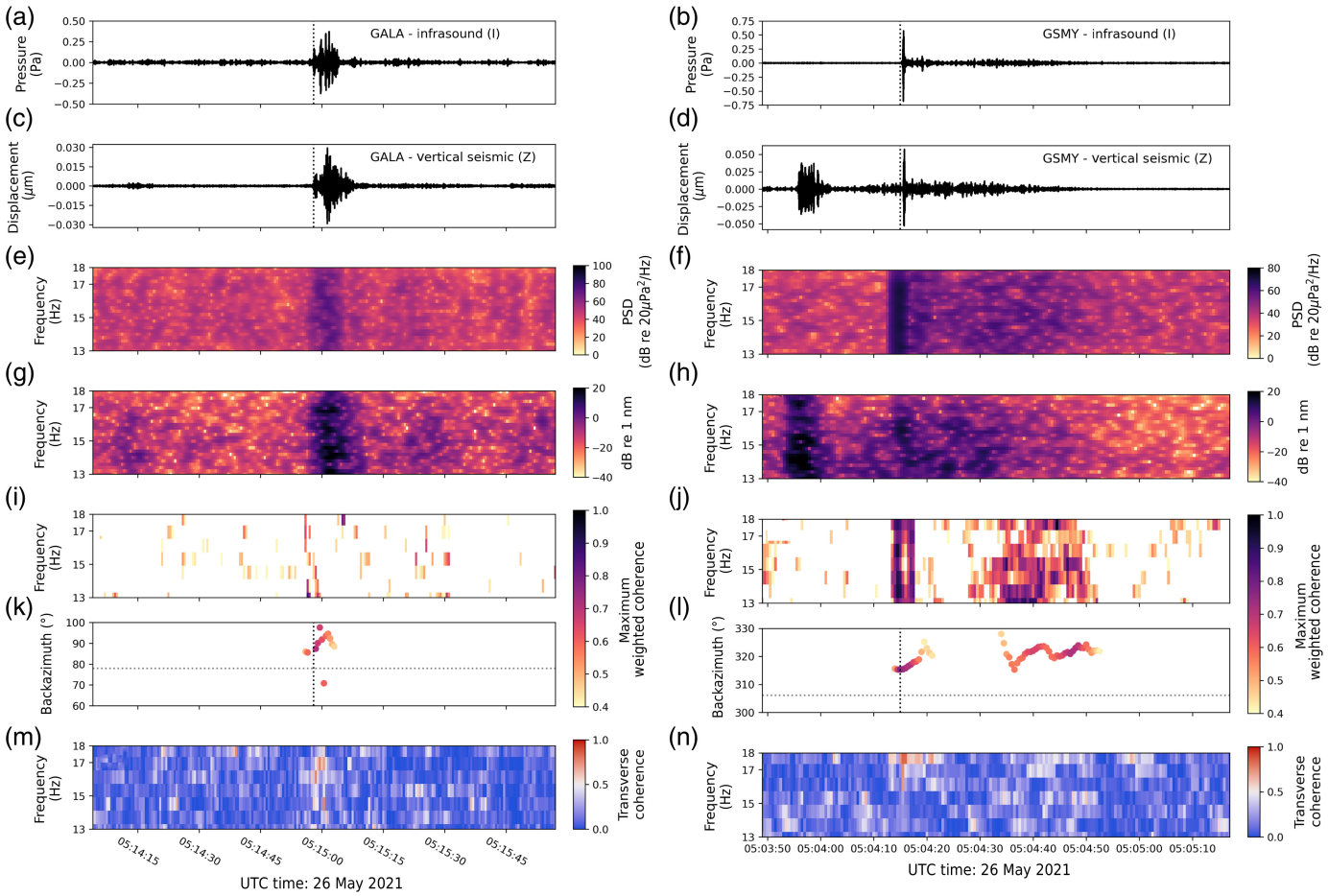

Figure 4. TCM analysis of the 26 May 2021 eruption of Great Sitkin Volcano recorded on AVO seismoacoustic stations GALA (a,c,e,g,i,k, m) and GSMY (b,d,f,h,j,l,n). The plot is organized in the same way as Figure 3.

Great Sitkin Volcano, but there is large variability (71°–98° for $C_{ZI} > 0.60$). For our 5 s windows, some back-azimuth values for the GCA are flipped 180°. However, increasing the window length used for processing appears to stabilize the back-azimuth estimates (see the supplemental material). The transverse coherence during the signal (Fig. 4m) varies broadly, but frequencies of high transverse magnitude-squared coherence appear to occur with low vertical magnitude-squared coherence (Fig. 4i,m).

Local station GSMY recorded an impulsive infrasonic signal at ~05:04:15 UTC followed by an ~30 s coda (Fig. 4b). The seismometer recorded both the coeruptive seismic signal at ~05:03:56 UTC followed by the impulsive GCA at the arrival time of the infrasound wave (Fig. 4d). Both the GCA and coda have high energy and coherence (Fig. 4f,j). The resulting back-azimuth estimate is shown in Figure 4l with the geographic back-azimuth (307°) to Great Sitkin Volcano. The back-azimuth estimates of the GCA are ~315°, with the back-azimuth (315°) at peak vertical magnitude-squared coherence ($C_{ZI} = 0.77$) deviated from the back-azimuth to Great Sitkin Volcano by ~9°. The transverse magnitude-squared coherence during this time is low, except for a brief period during the GCA at high frequencies (>17.0 Hz, Fig. 4n).

Infrasound and GCA signals recorded at regional stations KOWE and KONW are more emergent, and arrive at ~05:10:21 UTC and 05:10:33 UTC, respectively (Fig. 5a–d). Both the infrasonic signals are broadband (Fig. 5e,f) and have a coherent coda following the peak amplitudes (Fig. 5i,j). The back-azimuth estimates for KOWE are variable (Fig. 5k), ranging from 260° to 264° for vertical magnitude-squared coherence values greater than 0.80. At peak vertical coherence ($C_{ZI} = 0.90$), the estimated back-azimuth is 261°, which is deviated ~4° from the back-azimuth to Great Sitkin Volcano. The coda recorded at this station has lower coherence (peaking at 0.71) and varies from 280° to 256°. At the

Downloaded from http://pubs.geoscienceworld.org/ssa/tsr/article-pdf/3/4/249/5979003/tsr-2023023.1.pdf
by guest

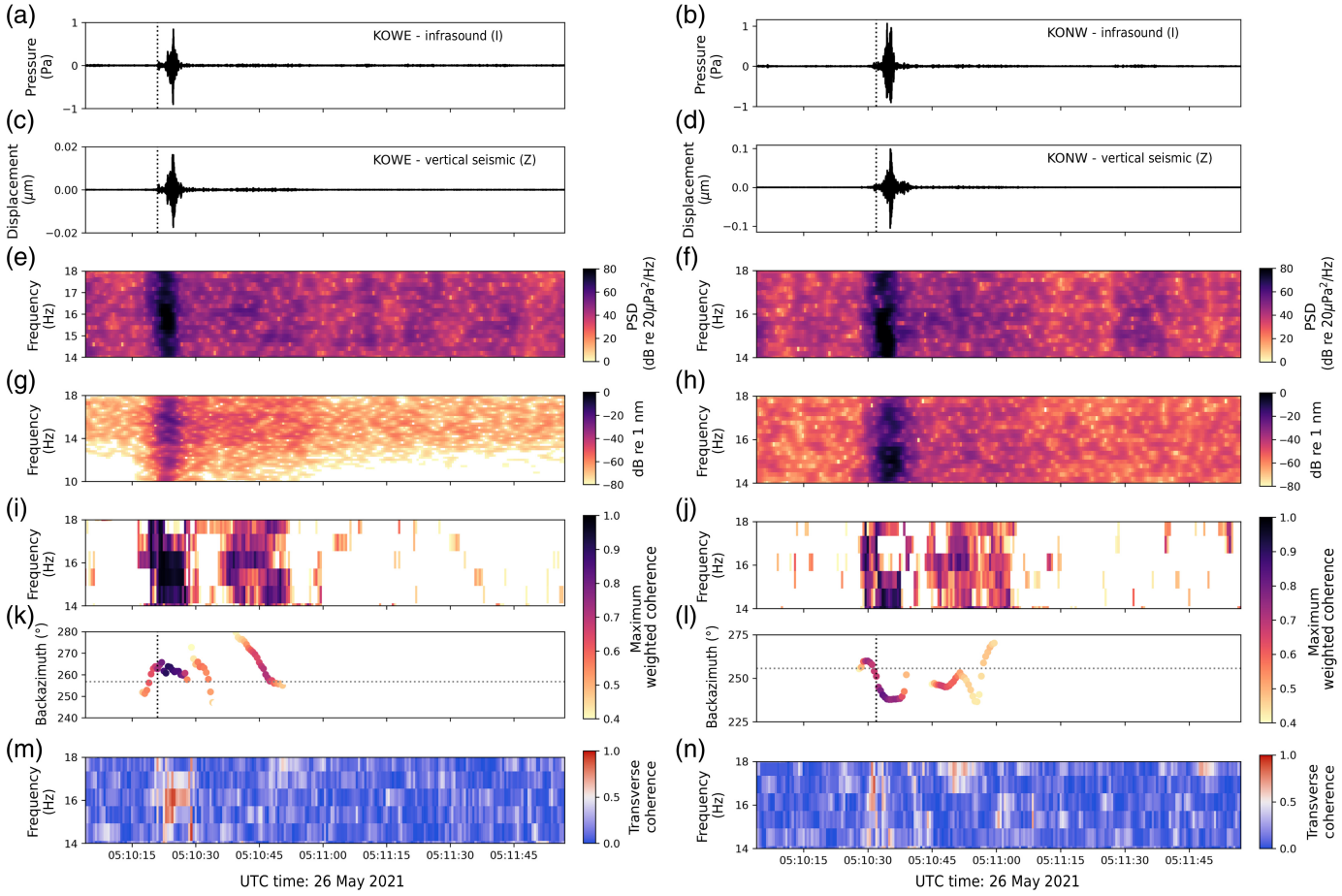

Figure 5. TCM analysis of the 26 May 2021 eruption of Great Sitkin Volcano recorded on AVO seismoacoustic stations KOWE (a,c,e,g,i,k,m) and KONW (b,d,f,h,j,l,n). The plot is organized in the same way as Figures 3 and 4.

maximum coherence ($C_{ZI} = 0.71$), the coda back-azimuth is approximately the same as the main signal (260°). The back-azimuth estimates for KONW are also variable (Fig. 5l), migrating between ~260° and 238°. The back-azimuth estimates sweep through the back-azimuth to Great Sitkin Volcano near the signal onset, but the back-azimuth estimate is 241° at peak coherence ($C_{ZI} = 0.83$). This value is deviated by ~15° from the back-azimuth to Great Sitkin Volcano. The acoustic coda has a lower overall coherence (peaking at $C_{ZI} = 0.66$) with back-azimuth estimates between 245° and 253° until migrating north with decreasing coherence. Despite having broadband coherence (Fig. 5i,j), both KONW and KOWE have relatively high transverse coherence at various frequencies (Fig. 5m,n).

Discussion

TCM processing expands the set of sensor configurations for infrasound signal back-azimuth estimation beyond conventional infrasound arrays or spatially separated seismoacoustic sensor pairs. This allows us to take advantage of existing colocated sensor pairs, such as the former TA, to obtain more back-azimuth estimates for signals of interest. We find that TCM can accurately estimate back azimuths at local (a few kilometers) to regional (tens to hundreds of kilometers) distances, although there is some variability in the back-azimuth estimates.

Detailed propagation modeling is beyond the scope of this article, but we can calculate celerities for the infrasound signals to better understand the propagation paths for the different GCAs. Using the explosion source time and distances between TA 121A and HRR-1 (160 km) and HRR-3 (173 km), we estimate celerities of 0.282 and 0.289 m/s for the impulsive arrivals in Figure 3a,b. These celerities suggest a stratospheric propagation path (Ceranna *et al.*, 2009). However, for these source–receiver distances, these arrivals are perhaps partial refractions from stratospheric altitudes, as noted in the previous analysis

Downloaded from http://pubs.geoscienceworld.org/ssa/tsr/article-pdf/3/4/249/5979003/tsr-2023023.1.pdf
by guest

for the HRR explosions (Green *et al.*, 2018). For the eruption of Great Sitkin Volcano, we use the visually picked arrival times of the infrasound waves at GALA (185 km), GSMY (6.5 km), KOWE (132 km), and KONW (136 km) to calculate infrasound celerities. These values are 0.279, 0.333, 0.344, and 0.343 km/s, respectively. These celerities suggest that the arrival at GALA is ducted through the stratosphere, the signal at GSMY is a direct arrival, and the signals at KOWE and KONW are ducted through the troposphere (Ceranna *et al.*, 2009). These propagation paths will intersect the ground surface at different incidence angles (Matoza *et al.*, 2011), which affects the apparent speed of the propagating acoustic wave and the coupling characteristics (Anthony, Ringler, *et al.*, 2022; Bishop *et al.*, 2022).

Both TCM analysis of the HRR-1 and HRR-3 explosion signals (Fig. 3) had less than ∼3° deviation between their back-azimuth estimates at peak coherence and the back-azimuth to their source locations. TCM processing of the Great Sitkin Volcano eruption data, however, displayed wide variability in back-azimuth estimates, with deviations between ∼4° and 20°. Some of this apparent back-azimuth variability with time may be due to our choice of window length and interaction of the acoustic coda with background noise. We uniformly used 5 s windows for processing throughout this article, but this choice may not be optimal for all the signal arrivals. One strategy to mitigate these effects would be to adapt the TCM method to a narrowband, adaptive window approach (Iezzi *et al.*, 2022). Back-azimuth deviation in the GSMY estimates (9.2°) is possibly due to propagation effects related to the local terrain (6.5 km distance). Large (≥10°) back-azimuth deviations from infrasound array processing calculations have also previously been reported after propagation over distances greater than 100 km (Matoza *et al.*, 2011; Green *et al.*, 2018; Dannemann Dugick *et al.*, 2022) as a result of atmospheric cross winds (Diamond, 1963) and concurrent arrival of multiple acoustic wavefronts (Green, 2015).

In addition to factors resulting from the acoustics, ground motion related to local geology (Anthony, Watzak, *et al.*, 2022; Wills *et al.*, 2022) may also impact TCM estimates. Notably, stations KOWE and KONW are located ∼4.4 km apart (Fig. 2). Infrasound peak-to-peak amplitudes are approximately the same at each sensor, but seismic displacements are only one-fifth as large at KOWE (0.2 μm) compared to KONW (1.0 μm). Station KOWE had not only a higher coherence between the infrasound and vertical seismic data than KONW (0.90–0.83), but it also had higher transverse coherence, specifically at 16 Hz. The transverse spectrograms for 121A, GALA, GSMY, KOWE, and KONW are calculated using the ground-truth back-azimuth to rotate the full length of seismic data. In contrast to signals at station 121A (Fig. 3g,h), stations GALA, GSMY, KOWE, and KONW all clearly show some energy on the transverse component (Figs. 4g,h and 5g,h). In fact, station GALA shows larger displacement on its horizontal components (N and E) than its vertical component (Z; see the supplemental material). High transverse energy has previously been noted from GCAs (Wills *et al.*, 2022), which is not predicted by current analytical models that assume a homogeneous half-space and flat terrain (Sorrells, 1971; Ben-Menahem and Singh, 1981). Our method also uses the assumption of retrograde particle motion to choose between the two candidate GCA back azimuths. Prograde ground motion has occasionally been observed for GCAs (Langston, 2004; Wills *et al.*, 2022), which would result in a 180° back-azimuth difference relative to the retrograde back-azimuth. For completeness, both the directions could be checked when using TCM results in an association algorithm (Matoza *et al.*, 2017; Blom *et al.*, 2020). A brief comparison of TCM results with seismic polarization analysis (Haney *et al.*, 2020) is presented in the supplemental material.

Systematic processing and infrasound propagation modeling is required to better understand the effects of seismoacoustic sensor installation on parameter estimates. TCM does not rely on time shifts, so there is not a strict minimum distance requirement between sensors. The practical outer limit for sensor pair distances also remains to be resolved, and may be some function of the frequencies of interest and the local noise field. Evidence from infrasound array processing suggests that coherence loss with increasing sensor separation is anisotropic (Green, 2015), and previous seismoacoustic work has shown that seismometers in boreholes have lower coherence with infrasound sensors than shallower burials (Ichihara, 2016; Anthony, Watzak, *et al.*, 2022). We also note in passing that any misalignment of the seismometer with respect to the cardinal directions would also result in a biased back-azimuth estimate, in which this bias is the rotation offset. Future work with propagation modeling might further illuminate the relative amounts of back-azimuth deviation due to propagation paths through the atmosphere and local coupling effects.

Conclusions

The TCM method adds to a growing suite of analysis methods for seismoacoustic data by providing an alternative approach to compute the back-azimuth of an infrasonic wave that is

Downloaded from http://pubs.geoscienceworld.org/ssa/tsr/article-pdf/3/4/249/5979003/tsr-2023023.1.pdf
by guest

recorded on an infrasound microphone and a seismometer. The resulting back-azimuth estimates from colocated sensors point in the direction of their source but are deviated to varying levels (1°–15°). These encouraging results suggest that the method could be applied to determine the back-azimuth from a variety of infrasound signals at difference source–receiver ranges. We assume that the particle motion is retrograde to determine the back-azimuth, but prograde ground motion from GCAs is possible (e.g., Langston, 2004; Bishop *et al.*, 2022; Wills *et al.*, 2022), which would lead to a 180° offset in the back-azimuth. Additional computational and experimental work are needed to further develop these methods. For example, our broadband analysis could be extended to a narrowband analysis (Iezzi *et al.*, 2022), which may be more appropriate for capturing frequency-dependent changes within a signal. It might also be necessary to record GCAs with a variety of sensor pair separation distances and geometries to determine optimal configurations for signals of interest, with deployment of seismometers at existing infrasound arrays being one approach (Gibbons *et al.*, 2015).

Data and Resources

This work made extensive use of ObsPy (Beyreuther *et al.*, 2010), and Figure 2 was created using PyGMT (Uieda *et al.*, 2022). All infrasound and seismic data analyzed in this work are available on EarthScope at https://ds.iris.edu/ds under network codes TA for station 121A and AV for the other stations. The Python transverse coherence minimization method (TCM) software is available on Github at https://github.com/uafgeotools/tcm. All websites were last accessed in August 2023. The supplemental material is a single pdf with supplemental text and figures.

Declaration of Competing Interests

The authors acknowledge that there are no conflicts of interest recorded.

Acknowledgments

The authors thank David N. Green for a helpful discussion about the results of Wills *et al.* (2022). The authors also thank Editor-in-Chief Keith D. Koper, Steven J. Gibbons, Ashton Flinders, and an anonymous reviewer for suggestions that improved the quality of this article. This work was supported by the Nuclear Arms Control Technology program at Defense Threat Reduction Agency under Contract Number HQ003421F0112. Approval for public release and the distribution is unlimited. This work was supported by the U.S. Department of Energy through the Los Alamos National Laboratory (LANL). LANL is operated by Triad National Security, LLC, for the National Nuclear Security Administration of U.S. Department of Energy (Contract Number 89233218CNA000001). This work was partially funded through U.S. Geological Survey (USGS) Cooperative Agreement Number G21AC10384 at the Alaska Volcano Observatory (AVO). Any use of trade, firm, or product names is for descriptive purposes only and does not imply endorsement by the U.S. Government. Robin S. Matoza acknowledges National Science Foundation (NSF) Grant Number EAR-1847736.

References

Anthony, R. E., A. T. Ringler, T. Tanimoto, R. S. Matoza, S. De Angelis, and D. C. Wilson (2022). Earth's upper crust seismically excited by infrasound from the 2022 Hunga Tonga–Hunga Ha'apai eruption, Tonga, *Seismol. Res. Lett.* **94,** no. 2A, 603–616.

Anthony, R. E., J. Watzak, A. T. Ringler, and D. C. Wilson (2022). Characteristics, relationships and precision of direct acoustic-to-seismic coupling measurements from local explosions, *Geophys. J. Int.* **230,** no. 3, 2019–2035.

Assink, J. D., G. Averbuch, P. S. M. Smets, and L. G. Evers (2016). On the infrasound detected from the 2013 and 2016 DPRK's underground nuclear tests, *Geophys. Res. Lett.* **43,** no. 7, 3526–3533.

Ben-Menahem, A., and S. J. Singh (1981). *Seismic Waves and Sources*, Springer, New York, New York, U.S.A.

Beyreuther, M., R. Barsch, L. Krischer, T. Megies, Y. Behr, and J. Wassermann (2010). ObsPy: A python toolbox for seismology, *Seismol. Res. Lett.* **81,** no. 3, 530–533, doi: 10.1785/gssrl.81.3.530.

Bishop, J., D. Fee, R. Modrak, C. Tape, and K. Kim (2022). Spectral element modeling of acoustic to seismic coupling over topography, *J. Geophys. Res.* **127,** no. 1, e2021JB023142, doi: 10.1029/2021JB023142.

Blom, P., G. Euler, O. Marcillo, and F. Dannemann Dugick (2020). Evaluation of a pair-based, joint-likelihood association approach for regional infrasound event identification, *Geophys. J. Int.* **221,** no. 3, 1750–1764.

Busby, R. W., and K. Aderhold (2020). The Alaska transportable array: As built, *Seismol. Res. Lett.* **91,** no. 6, 3017–3027.

Ceranna, L., A. Le Pichon, D. N. Green, and P. Mialle (2009). The Buncefield explosion: A benchmark for infrasound analysis across central Europe, *Geophys. J. Int.* **177,** no. 2, 491–508.

Dannemann Dugick, F. K., P. S. Blom, B. W. Stump, C. T. Hayward, S. J. Arrowsmith, J. C. Carmichael, and O. E. Marcillo (2022). Evaluating the location capabilities of a regional infrasonic network in Utah, US, using both ray tracing-derived and empirical-derived celerity-range and back-azimuth models, *Geophys. J. Int.* **229,** no. 3, 2133–2146.

Diamond, M. (1963). Cross wind effects on sound propagation, *J. Appl. Meteorol.* **3,** no. 2, 208–210.

Dybing, S. N., A. T. Ringler, D. C. Wilson, and R. E. Anthony (2019). Characteristics and spatial variability of wind noise on

Downloaded from http://pubs.geoscienceworld.org/ssa/tsr/article-pdf/3/4/249/5979003/tsr-2023023.1.pdf
by guest

near-surface broadband seismometers, *Bull. Seismol. Soc. Am.* **109,** no. 3, 1082–1098.

Edwards, W., D. Eaton, P. McCausland, D. ReVelle, and P. Brown (2007). Calibrating infrasonic to seismic coupling using the Stardust sample return capsule shockwave: Implications for seismic observations of meteors, *J. Geophys. Res.* **112,** no. B10, 10,306.

Fee, D., M. Haney, R. Matoza, C. Szuberla, J. Lyons, and C. Waythomas (2016). Seismic envelope-based detection and location of ground-coupled airwaves from volcanoes in Alaska, *Bull. Seismol. Soc. Am.* **106,** no. 3, 1024–1035.

Gibbons, S. J., T. Kværna, and S. Mykkeltveit (2015). Could the IMS infrasound stations support a global network of small aperture seismic arrays? *Seismol. Res. Lett.* **86,** no. 4, 1148–1159.

Green, D. N. (2015). The spatial coherence structure of infrasonic waves: Analysis of data from International Monitoring System arrays, *Geophys. J. Int.* **201,** no. 1, 377–389.

Green, D. N., R. Waxler, J.-M. Lalande, D. Velea, and C. Talmadge (2018). Regional infrasound generated by the Humming Roadrunner ground truth experiment, *Geophys. J. Int.* **214,** no. 3, 1847–1864.

Haney, M. M., D. Fee, K. F. McKee, J. J. Lyons, R. S. Matoza, A. G. Wech, G. Tepp, C. Searcy, and T. D. Mikesell (2020). Co-eruptive tremor from Bogoslof volcano: Seismic wavefield composition at regional distances, *Bull. Volcanol.* **82,** no. 2, 18.

Ichihara, M. (2016). Seismic and infrasonic eruption tremors and their relation to magma discharge rate: A case study for sub-Plinian events in the 2011 eruption of Shinmoe-dake, Japan, *J. Geophys. Res.* **121,** no. 10, 7101–7118.

Ichihara, M., M. Takeo, A. Yokoo, J. Oikawa, and T. Ohminato (2012). Monitoring volcanic activity using correlation patterns between infrasound and ground motion, *Geophys. Res. Lett.* **39,** no. 4, 4304.

Iezzi, A. M., R. S. Matoza, J. W. Bishop, S. Bhetanabhotla, and D. Fee (2022). Narrow-band least-squares infrasound array processing, *Seismol. Res. Lett.* **93,** no. 5, 2818–2833.

Johnston, A. C. (1987). Air blast recognition and location using regional seismographic networks, *Bull. Seismol. Soc. Am.* **77,** no. 4, 1446–1456.

Kim, K., and A. Rodgers (2017). Influence of low-altitude meteorological conditions on local infrasound propagation investigated by 3-D full-waveform modeling, *Geophys. J. Int.* **210,** no. 2, 1252–1263.

Langston, C. A. (2004). Seismic ground motions from a bolide shock wave, *J. Geophys. Res* **109,** no. B12, doi: 10.1029/2004JB003167.

Matoza, R. S., and D. Fee (2014). Infrasonic component of volcano-seismic eruption tremor, *Geophys. Res. Lett.* **41,** no. 6, 1964–1970.

Matoza, R. S., D. N. Green, A. Le Pichon, P. M. Shearer, D. Fee, P. Mialle, and L. Ceranna (2017). Automated detection and cataloging of global explosive volcanism using the international monitoring system infrasound network, *J. Geophys. Res.* **122,** no. 4, 2946–2971.

Matoza, R. S., A. Le Pichon, J. Vergoz, P. Herry, J.-M. Lalande, I.-H. Lee, I.-Y. Che, and A. Rybin (2011). Infrasonic observations of the June 2009 Sarychev Peak eruption, Kuril Islands: Implications for infrasonic monitoring of remote explosive volcanism, *J. Volcanol. Geotherm. Res.* **200,** no. 1, 35–48.

McKee, K., D. Fee, M. Haney, R. Matoza, and J. Lyons (2018). Infrasound signal detection and back azimuth estimation using ground-coupled airwaves on a seismoacoustic sensor pair, *J. Geophys. Res.* **123,** no. 8, 6826–6844.

Mendo-Pérez, G., A. Arciniega-Ceballos, R. S. Matoza, A. Rosado-Fuentes, R. W. Sanderson, and B. A. Chouet (2021). Ground-coupled airwaves template match detection using broadband seismic records of explosive eruptions at Popocatépetl volcano, Mexico, *J. Volcanol. Geotherm. Res.* **419,** 107,378.

Sorrells, G. (1971). A preliminary investigation into the relationship between long-period seismic noise and local fluctuations in the atmospheric pressure field, *Geophys. J. Int.* **26,** nos. 1/4, 71–82.

Uieda, L., D. Tian, W. J. Leong, M. Jones, W. Schlitzer, M. Grund, L. Toney, J. Yao, Y. Magen, K. Materna, *et al.* (2022). PyGMT: A python interface for the generic mapping tools, Zenodo, doi: 10.5281/zenodo.6702566.

Wills, G., A. Nippress, D. Green, and P. Spence (2022). Site-specific variations in air-to-ground coupled seismic arrivals from the 2012 October 16 explosion at Camp Minden, Louisiana, United States, *Geophys. J. Int.* **16,** no. 1, 243–255.

Manuscript received 16 June 2023
Published online 2 October 2023

Downloaded from http://pubs.geoscienceworld.org/ssa/tsr/article-pdf/3/4/249/5979003/tsr-2023023.1.pdf
by guest